Design and Performance Test of a Prototype MRI-Compatible Cascaded Pressure Microsensor

L. Arntzen[1], M. van der Hoek[2], U. Wyder[3], D. Boesten[4], J. Schreuder[5], J. Bolte[6]

[1]Smart Sensor Systems, THUAS, Delft, NL

[2]Van der Hoek Photonics. Vlaardingen, NL

[3]Fontys University Eindhoven, NL

[4]Smart Sensor Systems, THUAS, Delft, NL

[5]CDLeycom, Hengelo, NL

[6]Smart Sensor Systems, THUAS, Delft, NL

DOI: https://doi.org/10.51584/IJRIAS.2026.11030086

Received: 21 March 2026; Accepted: 26 March 2026; Published: 14 April 2026

ABSTRACT

In this paper, the design, simulation, fabrication and characterization of a prototype single fiber MRI compatible cascaded pressure sensor is presented. This paper represents the extended version of earlier communication on this topic. In addition to the earlier communication, in this paper, we report on a crucial design requirement: the immunity to Electro-Magnetic Interference (EMI). This immunity has been experimentally tested by combining the prototype sensors with a Siemens 1.5T Magnetic Resonance Imaging (MRI) apparatus at Haga Hospital (The Hague). No disturbance was observed during a full MRI imaging cycle. The system allows for long lasting usage in the range -50 mmHg to 300 mmHg without damage to the membrane. A static pressure resolution (averaged over the array) of 3.6 mmHg was found, a performance that needs improvement in the future. Simulations show that the desired resolution of 1.0 mmHg is feasible within this design approach. The dynamical response allows for registration of dynamical features up to 20 Hz, already meeting dynamical requirements of this low-cost sensing system and already exceeding expectations expressed in advance. Future work includes further miniaturization, catheter integration, improvement of static pressure resolution, tackling separation of temperature-pressure crosstalk by implementing alternating independent Fibre Bragg Grating (FBG) temperature sensors in the array and further enhancing dynamical properties.

Keywords: Photonic Integrated Circuit; Microring Resonator (MRR); Cardiovascular diseases; Cardiac Performance; Cascaded Blood Pressure Sensor; MRI-compatible; Optical Fiber Array; Catheter; Fiber Bragg Grating, Electro Magnetic Interference (EMI).

INTRODUCTION

In the Netherlands alone, ~230.000 reported hospitalizations due to cardiovascular disease are reported every year [14]. A total number of ~36.000 people casualties are registered yearly as a result of cardiovascular disease, representing 22% of the total mortality. For the diagnosis and prevention of cardiovascular disease, measurements of cardiac performance are of considerable importance. To improve diagnostics, accurate and reliable measurements are critical; for example, to determine cardiac output, Pressure-Volume (PV) curves are often measured with piezo-based pressure sensor arrays on a catheter tip. Measuring pressure in an array allows for measuring other important local medical indicators, such as the Fractional Flow Reserve (FFR) [15]. These indicators are essential for medical diagnosis, and are currently standard procedure. However, one of the central problems of piezo sensors is that this detection technique is based on electrical signals, which limits precision and reliability due to static magnetic fields and EMI. Moreover, it is highly desirable, that future

ISSN No. 2454-6194 | DOI: 10.51584/IJRIAS |Volume XI Issue III March 2026

detection techniques can combine diagnostic capabilities with MRI [17]. This implies that the performance of the sensor must be independent of magnetic fields, preferably up to 7 T [18]. The sensing should be independent of EMI during a complete MRI cycle. In order to tackle this, an approach was chosen to combine the fabrication of a pressure membrane on the micro scale with the application of integrated optics [16]. More generally stated, combining fabrication on the micro scale with integrated optics opens the possibility for the development of a whole new generation of catheter sensors. In addition to the immunity for EMI requirement, it is desired that the sensor is suitable for catheters with a diameter of 5 Fr (1,67 mm) and a pressure resolution should be 1 mmHg or less. The sensing system is required to operate in the range -50 mmHg to 300 mmHg, since negative pressures are common in the blood stream. The dynamical response should allow registration of features in the pressure-time curves with a minimum of 10 Hz.

In section II, an overview of relevant literature is presented, and in section III the presented simulation reveals the potential sensitivity of the sensor design. In section IV details concerning the microfabrication of the sensor are discussed. In section V the details concerning the measurement setup are discussed.

BACKGROUND AND LITERATURE

The strategy for ruling out EMI during sensing is based on applying a single optical fiber consisting of multiple FBGs separated by any adjustable spacing. Combined with an interrogator, the FBGs measure a shift in near-infrared electromagnetic wavelength proportional to the deformations of a Silicon Nitride (Si_3N_4) membrane at varying pressures. FBG's already have a long history, dating back to 1978 [2]. The amount of applications has been growing rapidly in a wide field, for example in telecommunication, optical sensing, particle physics experiments, structural health monitoring, including buildings and bridges [3], maintenance of machines [6], biomedical diagnostics [16], and more. FBGs are constructed by exposing the (light sensitive) core of an optical fiber to ultra-violet radiation in a periodic pattern. Due to the UV radiation the refractive index of the core changes, thus creating a Bragg reflector. If strain is applied to this fiber, the Bragg condition shifts, inducing the shift of reflected radiation to longer wavelength. In this way an optical strain detector is created. FBGs have many advantages over conventional sensing systems, in many cases involving electrical signals. This makes the FBG technique well suited for measuring in a clean and undisturbed way, even under harsch conditions. These Bragg reflectors are also fabricated in an array within a single fiber. Such an array of Bragg reflectors leads to yet another series of interesting applications: low-cost interrogation systems, real-time monitoring of subsurface pressure-waves in a water tank [4], multi-point monitoring of mechanical structure, such as airplane wings, and many more. Medical applications are emerging too, using an array of FBGs, such as an catheters for the diagnosis of gastrointestinal motility disorder [5]. These arrays are of added value due to their phase sensitivity, individual read out and the possible dynamical properties of the measuring system. For clarification of possible future applications of fiber arrays, we will first describe some background in fluid dynamics. In fluid dynamics, the most simple form of Bernoulli's Law states

$$P + \frac{1}{2}\rho v^2 = constant, \tag{1}$$

where P refers to the static pressure, and the second term refers to the dynamic pressure. This equation is easily derived directly from energy conservation. It implies that a cascade of micro scaled pressure sensors can be used to trace stenosis in a blood vessels, as visualized in ure 1. Poisseuille-Hagen law describes the pressure difference over a cylindrical tube of length L, of a fluid in laminar fluid flow

$$\Delta P = \frac{8\mu L Q}{A^2}, \tag{2}$$

where Q refers to the flow rate, A the cross-sectional area of the cylindrical tube, and μ [Pa · s] the dynamical viscosity. The assumptions in the derivations set some limitations using (1) and (2), but the equations are illustrative for additional applications of a cascaded micro scaled pressure sensor. This leads to the idea that such a fiber FBG array is suitable for verifying correct positioning of a stent after surgery - since correct stent

ISSN No. 2454-6194 | DOI: 10.51584/IJRIAS |Volume XI Issue III March 2026

positioning would directly cause reduction in blood pressure difference over the stenosis. More applications are feasible, since the proportion of red blood cells in the blood (hematocrit) correlates with the viscosity. An increase of hematocrit leads to a higher viscosity. On average, blood has a viscosity of approximately three times that of water, meaning that the driving pressure to pump blood through the vessels is higher. Polycythemia (or Erythrocytosis) is an anomaly leading to a enlarged hematocrit that can reach up to 70% [20]. The viscosity of the blood will then be up to ten times larger than that of water, making it harder for the heart to pump blood through the vascular system. Equation (2) shows that a cascade of pressure sensors fitted in a catheter show an abnormal pressure decline over the cascade. Additional diagnostic detection is possible, if the sensor cascade has sufficient dynamical response. In that case, it will be possible to analyze the arterial pulse in the time domain, revealing the performance of the heart and vessels [21]. The arterial pulse is created by the heart and blood in injected into the aorta. The wave shape depends on the ejection pressure pattern, but also on properties of large arteries, particularly on their stiffness. Waveform analysis in the time domain leads to crucial information valuable for diagnostics, comparable to the more familiar dynamical information on cardiac performance extracted from ElectroCardioGrams (ECGs). Extraction of other vital information on cardiac performance can be done by analyzing the pulse waveform. This can exceed basic information, such as heart pumping rate, and systolic and diastolic pressure measurement. In addition to the first example, monitoring stiffening of arteries, a second application example involves a direct real time measurement of the effect of drugs, which is still a medical challenge up until the present day. If the dynamics in pressure waves measurement is sufficient, the influence of an arterial vasodilator could be measured directly, the same accounts for the effect of Calcium Channel Blocking drugs (CCBs), Receptor Blockers (ARBs), and many more. A typical example of a study performed exploring pressure curves with a high precision, is shown in Figure 2. More details and examples are found in literature [21], and this shows that a dynamical resolution of ≈10 Hz, already will reveal important diagnostic information from the pressure wave.

Figure 1. Bernoulli states a direct relation between cross-sectional areas A_1 and A_2, static pressures P_1 and P_2 , and flow speeds v_1 and v_2 . If the area reduces,the static pressure reduces, while the dynamic pressure increases. This implies that a cascaded pressure sensor can be used to trace stenosis

Figure 2. Typical example of pressure time domain analysis. Analysing the exact shape and properties, can be used as an diagnostic tool. Adapted from: [21]

SIMULATION

To evaluate the crucial variables of the sensor design that influence its sensitivity, a Finite Element Modeling (FEM) simulation was conducted using a FEM model in COMSOL Multiphysics [27]. The model is shown in

ISSN No. 2454-6194 | DOI: 10.51584/IJRIAS |Volume XI Issue III March 2026

Figure 3, in which the green cylinder represents the fiber, the blue line the adhesive, and the pink rectangle the SiNi membrane. Multiple studies with different parameter sweeps were made in order to find the influence of the SiNi membrane thickness, width and length, adhesive properties, FBG positioning, and more. During manufacturing it is possible to select a desired SiNi membrane thickness. The influence of the thickness on the sensitivity was examined with a thickness of 200 nm and 400 nm. The fiber displacement was measured at applied pressures of 50 mmHg, 100 mmHg, and 200 mmHg. The results can be seen in Figure 4. At 200 mmHg, a fiber displacement of 249.6 nm was measured for the 200 nm thick membrane. For the 400 nm membrane, a

displacement of 210.9 nm was measured, which confirms that a thinner membrane leads to a higher sensitivity. UV-hardening adhesive can have a Young's modulus between 0,01 GPa and 3 GPa [26]. With a Young's modulus of 3 GPa the maximum deformation change the fiber experiences a displacement of 156 nm. With a Young's modulus of 1 GPa, the maximum deformation change the fiber achieves is displacement of 177 nm. This means a lower Young's modulus results in a higher sensitivity. However, The adhesive with a Young's modulus of 0,1 GPa or lower, the fiber begins to deform on top of the substrate. This could indicate that the fiber detaches from the substrate, meaning an optimum has to be found between maximum deformation and desired adhesion.

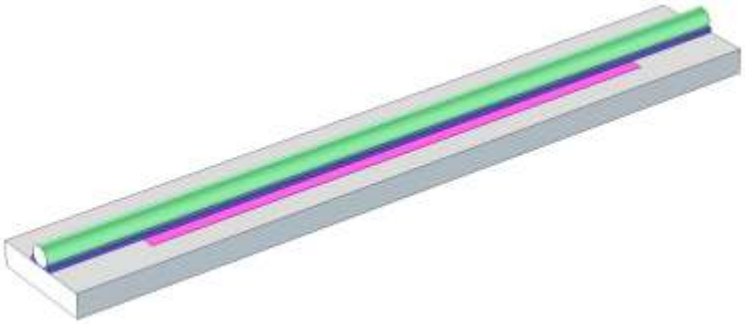

Figure 3. The Finite Element Model (FEM) that was used to find the influence of SiNi membrane thickness, adhesive properties, and more.

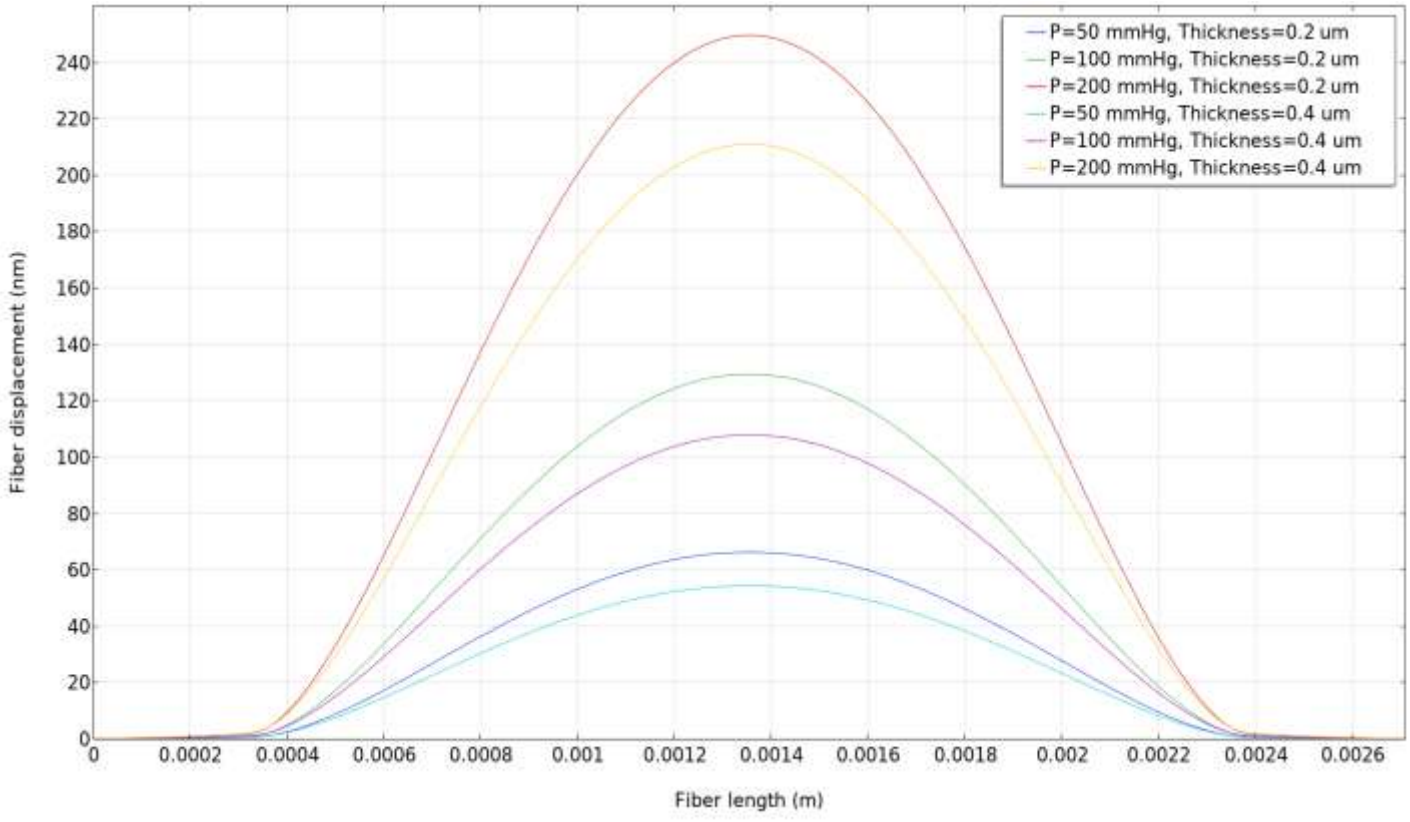

Figure 4. FEM results of the influence of membrane thickness on the sensitivity of the sensor.

ISSN No. 2454-6194 | DOI: 10.51584/IJRIAS |Volume XI Issue III March 2026

FABRICATION

The fabrication of the sensor device consists of the fabrication of the $Si_3 N_4$ membrane using photo-lithographic processes and the adhesion of the FBG to the Si_3N_4 membrane.

Microfabrication of the Silicon Nitride Membrane

For the micro fabrication of the Si_3N_4 membrane, a 300 μm double side polished p-type (boron) Silicon wafer with a <100> orientation is used. Using Low Pressure Chemical Vapour Deposition (LPCVD) with a mixture of NH_3 and H_2SiCl_2, a thin film of Si_3N_4 is deposited on both sides of the substrate. Si_3N_4 was chosen because of its relatively high flexibility and low etch rate compared to Silicon. The thickness of the deposited Si_3N_4 thin film was measured using an Woollam M-2000 Ellipsometer at a value of 399.47 nm. The stress of the thin film was measured with the use of a Flexus 2320-S thin-film stress measurement instrument at a value of 337.73 MPa. The wafer with a thin film of Si_3N_4 is shown in Figure 5, left. Using an ASML PAS 5500/60 stepper, rectangular patterns representing the membranes are exposed on a layer of photo resist that is deposited to the backside of the wafer. The exposed patterns are etched away using a Drytek Triode 384T plasma etcher with a mixture of 90% C_2F_6 and 10% Cl_2 until the bare silicon of the wafer remains. The resulting exposed patterns are shown in Figure 5, right. A cavity is created by placing the wafer in a bath of distilled water with 30% potassium hydroxide (KOH) until the silicon is completely etched and only the thin Si_3N_4 layer on the topside of the wafer remains. The silicon wafer with an orientation of <100> etches faster than in the <111> orientation, resulting in a V-shaped cavity with an angle of 54.7 degrees. The cavity, combined with the thin layer of Si_3N_4, acts as a pressure chamber that deforms dependent on the loading conditions. The Si_3N_4 membrane has dimensions of 2.0mmx0.3 mm. Lastly, the wafer is diced using a diamond saw resulting in rectangular chips with a size of 10x2.5x0.3 mm (LWH).

Adhesion of Silicon Nitride Membrane and FBG

As shown in Figure 4, the deformation of the Si_3N_4 membrane is the highest in the center of the membrane. Thus, it is important to align the FBG precisely at the center of the Si_3N_4 membrane. For this purpose, an alignment setup is made consisting of clamps for the optical fiber, a chip housing and an XYZ micro manipulator with a precision scale of 1.0 μm for the positioning of the optical fiber on top of the membrane. The chip housing is made using an Stereo-lithography (SLA) 3D printer, and is shown in Figure 6. The aligned optical fiber is bonded to the Si_3N_4 membrane using an UV-curable adhesive with low shrinkage properties [26].

Figure 5. Left: Wafer with a $S_{i3}N_4$ thin film. Right: Wafer with exposed patterns representing the membranes.

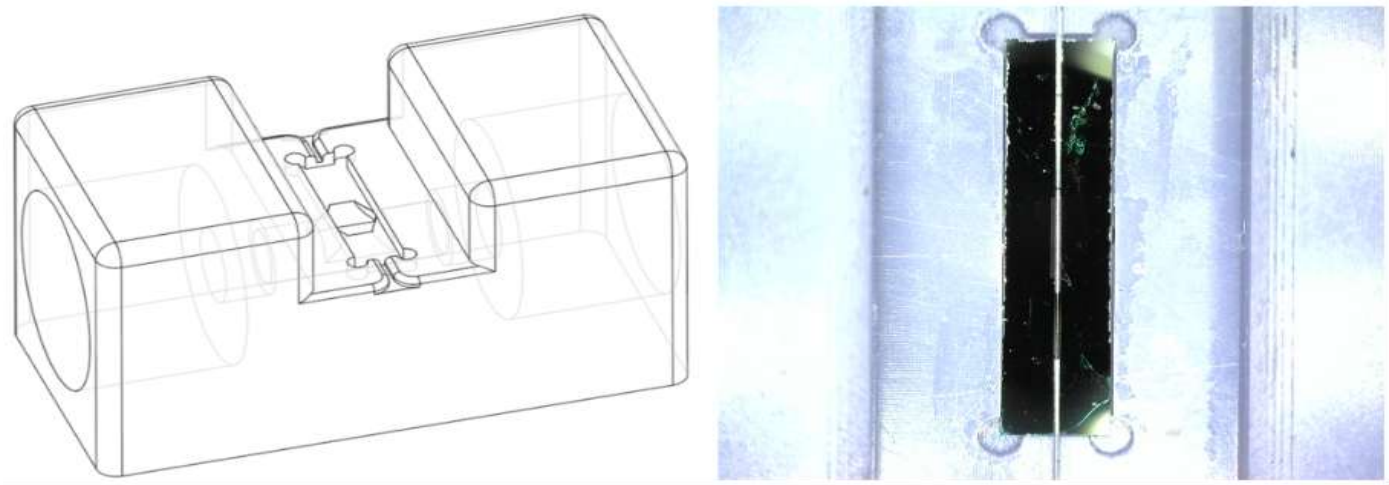

Figure 6. Left: CAD drawing of the chip housing. Right: 3D printed chip housing with an FBG aligned on top of the $Si_3 N_4$ membrane.

MEASUREMENT SETUP

The chip housing not only holds the rectangular chips with the Si_3N_4 membrane in place, but also has a built-in provision for Luer locks, for connecting pressure input and output hoses. The Luer locks allow multiple pressure sensors to be connected together so that pressure changes can be measured simultaneously at multiple points along the optical fiber. The measurement device with three fabricated pressure sensors in cascade is shown in Figure 8. The optical fiber is connected to a FAZT I4G interrogator that measures the wavelength shift of the FBGs at a measurement frequency of 2 kHz with resolution of 1 pm [25]. Blood pressure signals are generated with a Biotek Fluke 601A Blood Pressure System Calibrator connected to the pressure sensing cascade. This device, shown in Figure 9, is capable of emulating heart pressure rhythms in a range of systolic and diastolic blood pressure values and wave forms. The temperature dependence of the sensors were measured using a Luna Hyperion Si255 interrogator – the specifications of the FAZT I4G and the Luna Hyperion Si255 are comparable, and this was done due to availability of the interrogators.

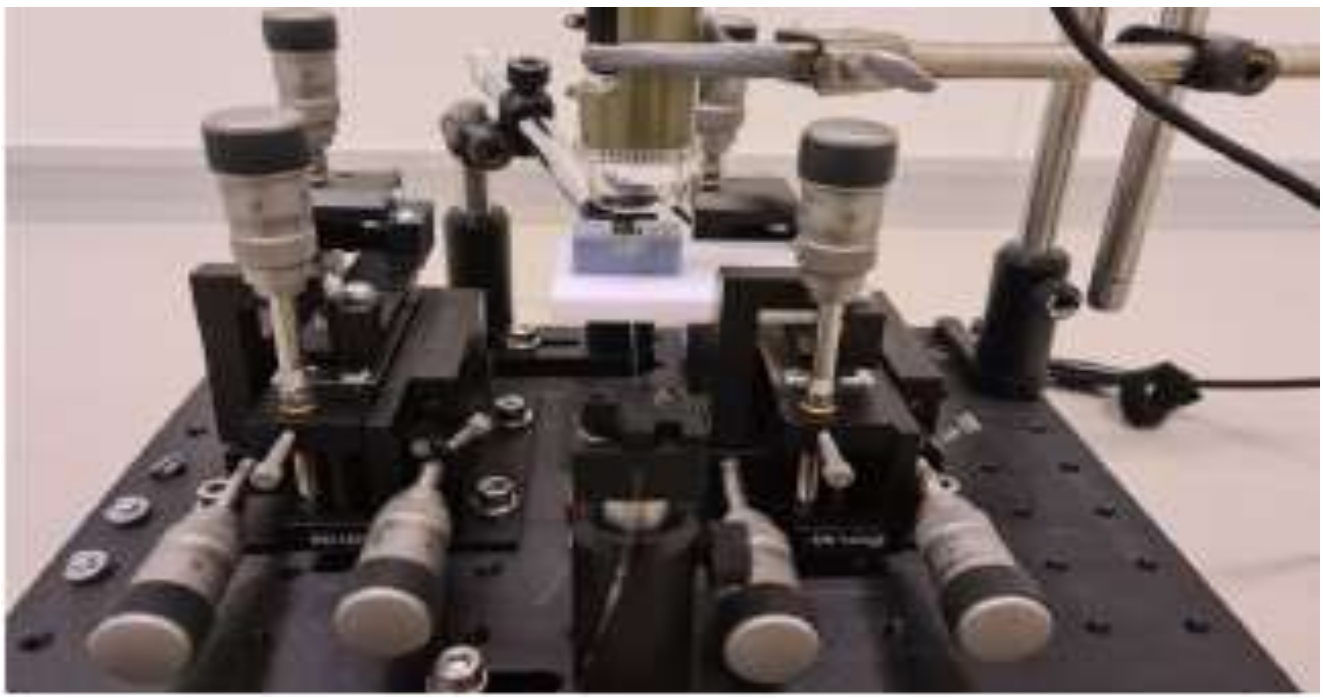

Figure 7. All FBG positions in the fibre are localized, and positioned using a 4-axis micropositioning unit in the middle of the fibre with an accuracy of 1 μm

ISSN No. 2454-6194 | DOI: 10.51584/IJRIAS |Volume XI Issue III March 2026

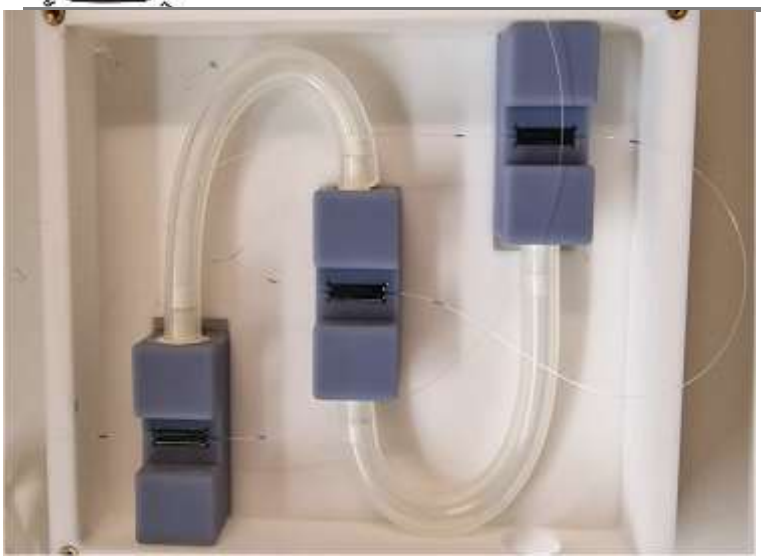

Figure 8. Measurement device consisting of three cascaded pressure sensors, each on a chip housing, with a single optical fiber

Figure 9. Biotek Fluke 601A Blood Pressure System Calibrator connected to the pressure sensing cascade. This device is capable of emulating heart pressure.

RESULTS AND DISCUSSION

The characteristics and performance of the fabricated cascaded blood pressure sensors were determined by applying various loading conditions and measuring the wavelength shift relative to a steady state at 0 mmHg.

Statical Pressure

The average statical wavelength shift of the three sensors is measured at a value of 0.83 ± 0.05 pm due to a pressure change of 60 mmHg. The sensor resolution of 3.6 mmHg of

the system, as already reported in earlier communication, this was already reported, is confirmed. Although 3.6 mmHg is a promising result, it does not yet meet the design requirement desired for the pressure resolution of 1 mmHg. Based on FEM simulations, future prototype sensors are expected to meet this requirement by tuning fabrication (glueing and FBG positioning), reduction of membrane thickness and enlarging membrane width and length.

Dynamical Pressure Response

An Atrial tachycardia heart rhythm at a systolic blood pressure of 140 mmHg and a diastolic blood pressure of 80 mmHg at a frequency of 120 BPM was applied to the sensor array. The rhythm was generated by a Biotek Fluke 601A Blood Pressure System Calibrator as shown in Figure 9, and the fiber was connected to a FAZT I4G interrogator. From Figure 10 and Figure 11, it becomes clear that the dynamical response of the sensors already exceeds the preset design requirement and dynamical features in the pressure wave up to 20 Hz (50 ms) are distinguishable. The performance is still limited by the dynamical specifications of the interrogator. This dynamical behavior enables a new range of medical diagnostic applications for this design.

Temperature Dependence

The averaged wavelength shift of the pressure sensors has been monitored during 120h with the fluid tubing disconnected. Figure 13 shows the result of temperature monitoring of temperature during the same period using a standard thermocouple Figure 14 shows the same data, but this time the wavelength shift as a function of temperature is plotted. From a linear fit, the wavelength shift as a function of temperature was extracted. This results in a temperature dependence of 62.7 ± 0.1 pm/K. The measurement reveals that crosstalk of temperature and pressure is not negligible for this design. Independent local temperature measurements for a robust separation of temperature and pressure measurements is required for future prototypes studies.

MRI Compatibility

In order to experimentally investigate the essential key requirement that the sensor system should be fully MRI compatible, the system was combined with a Siemens 1.5 T MRI apparatus at Haga Hospital (The Hague). As shown in Figure 12, the sensor cascade was positioned in the core of the MRI apparatus, localized at the default patient position. In Figure 15, the wavelength shift as a function of time is shown. During the time frame full MRI imaging cycles were applied, containing standard series of MRI pulses on top of the 1,5 T static magnetic field. The resulting wavelength shift due to a standard pressure pulse is compared with a second data set. In Figure 15 (below) this data set is shown, an identical pressure wave of 30 pm was applied, this time however, the sensor cascade is outside the MRI apparatus, at a position of near zero field. As expected, no measurable disturbing influence of both the DC magnetic field and the MRI pulses on top were found during MRI operation. Drift in pressure sensing during the complete data is found to be smaller than 7 pm, corresponding to a maximum temperature change of 0.1 K. Therefore, heating effects during the MRI operation are found to be negligible during these test measurements.

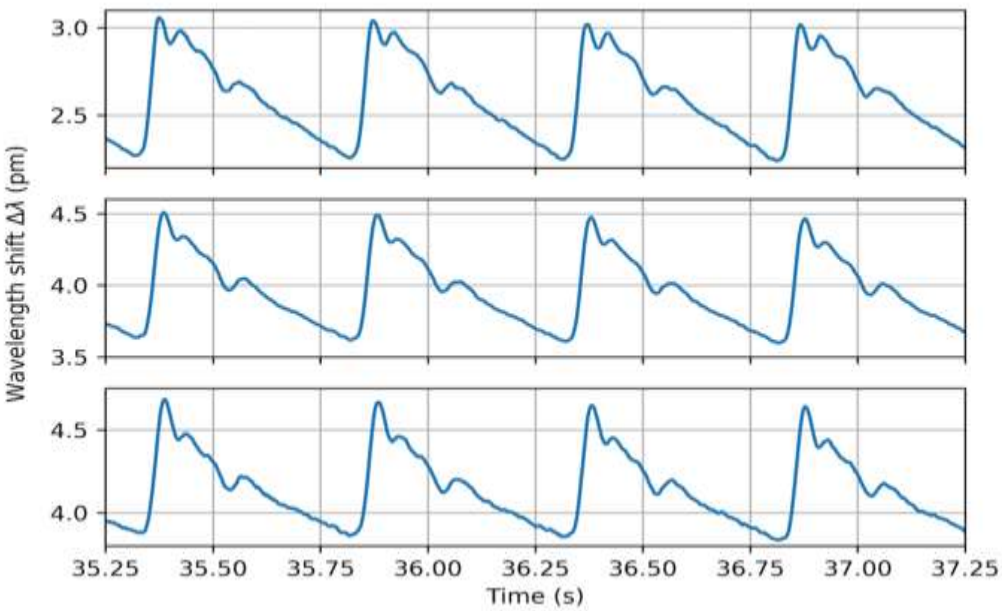

Figure 10. Performance of the cascaded pressure sensors on a single optical fiber. An Atrial tachycardia heart rhythm was emulated at a systolic blood pressure.

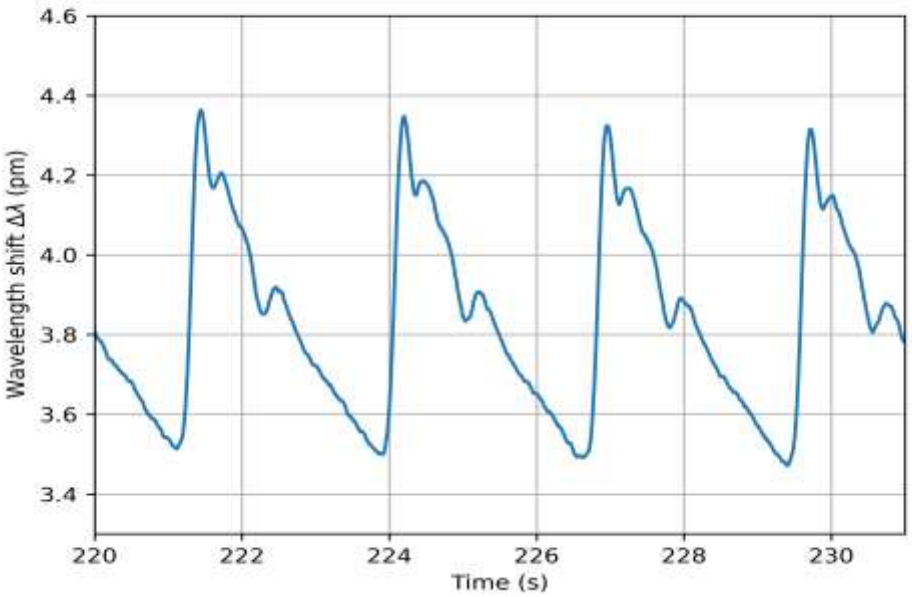

Figure 11. Biotek Fluke 601A Blood Pressure System Calibrator connected to the pressure sensing cascade. This device is capable of emulating heart pressure.

Figure 12. MRI apparatus in which the cascaded blood pressure sensor setup was placed.mance of the cascaded pressure sensors on a single optical fiber.

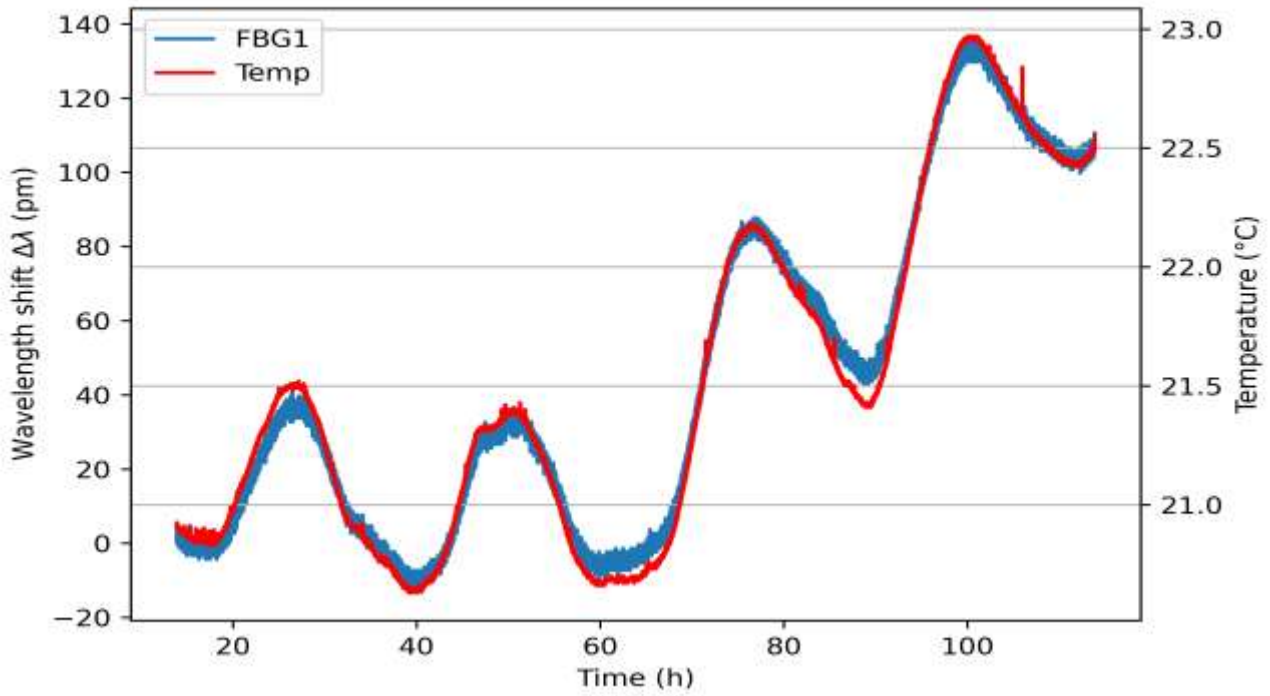

Figure 13. The basic output of the pressure sensor, wavelength shift (pm), independent temperature data logged during a period of 120 minutes

CONCLUSION AND FUTURE WORK

In this study, a prototype MRI-compatible cascaded blood pressure sensor suitable for catheterization was designed, simulated, fabricated and characterized. An operating pressure range from -50 mmHg to 300 mmHg has proven to be long lasting applicable for the sensing system without causing damage. The possibility of measuring negative pressures is of critical importance for medical applications, since it is a common feature in the blood stream, especially near and in the heart. Meeting this requirement ensures that the sensing system is suitable for common medical heart performance applications, i.e., PV-Loops, Corony Flow Reserve (CFR) and Fractional Flow Rate (FFR) measurements. The wavelength shift, for three cascaded sensors averaged, is measured at a value of 0.83 ± 0.05 pm as a result of a DC pressure step of 60 mmHg. An average sensor resolution of 3.6 mmHg is found independent of the applied interrogator resolution and is expected to be limited by the sensor itself. Future work is needed to improve the fabrication of the sensor itself in order to reach the required resolution of 1 mmHg. This can obviously be achieved by increasing the deformation of the Si_3N_4 membrane per unit pressure. FEM simulation shows that this can be done by increasing the width of the membrane, or by fabricating an even thinner SiNi membrane. FEM simulation also shows that a precise alignment of the FBG in the middle of the membrane is crucial for reaching this resolution. In the adhesive strategy, there is also room for improvement. The balance between young's modulus, adhesive type, and adhesive thickness can still be optimized further. Further reduction of the diameter of the FBG fiber array is another tuning parameter. For this prototype a diameter of 80 µm was used, leading to a cascaded sensing system of considerable robustness, manageable fabrication and adhesive strategy. FEM simulations show that reducing the diameter of the fiber improves the resolution, however, concerns for the robustness of the system will rise. Wider dimensions of the membrane therefore are for now the preferred candidate for future prototype studies, and simulations show that it is possible to meet the resolution requirement while using a 80 µm fiber. The dynamical response of the sensors was characterized by applying an emulated atrial tachycardia cardiac rhythm at a systolic blood pressure of 140 mmHg and a diastolic blood pressure of 80 mmHg at a frequency of 120 BPM, the results show that dynamical features up to 20 Hz (50ms) are distinguishable. The dynamic response measurements were performed using a FAZT I4G interrogator. The dynamic response of the system was shown to meet the requirement to show features up to 10 Hz (10 ms). We conclude that the dynamical

requirement for pressure sensing has been met for this prototype and is sufficient for observing dynamical diagnostic characteristics in the blood pressure wave. However, work has to be done in order to reduce the size of the sensor. The developed prototype has a width of 2,5 mm, and in order to achieve the desired diameter of 5 Fr (≈ 1,67 mm) or less, further miniaturization efforts are required to reduce the size of the chip containing the Si_3N_4 membrane, i.e., by reducing the size of the silicon substrate surrounding the membrane. This implies that we are challenged to enlarge the membrane size, while reducing the substrate size. The Dicing method determines the limiting factor for dimensions of this substrate. In the fabrication procedure, Blade Dicing was applied, resulting in a width of 2.5 mm. Other methods for dicing, such as laser Dicing, plasma dicing should be evaluated for future fabrication improvements. In addition, future work on the next prototype is planned on the integration of the sensor design into a catheter. In Figure 14 the shift in wavelength as a function of temperature is shown, and this result confirms that measuring pressure without interdependence with temperature is not feasible. The temperature dependence measurements (with the fluid pressure disconnected) leads to a wavelength shift dependence of 62.7 ± 0.1 pm/K. In a follow up project, one (or more) separate FBG(s) in the cascaded single FBG fiber will have to be calibrated for temperature only, i.e. temperature should be measured separately. The full dataset is then used to extract both temperature and pressure in a clean way. This data is also needed in order to monitor drift in pressure sensing. In addition, as described, the added temperature (cascaded) temperature sensors and pressure sensors combined also open up a wider range of diagnostic applications. In an earlier communication we showed the compatibility of the sensors in DC magnetic fields up to 1.3T. No measurements were done yet to verify compatibility with AC and DC fields used in MRI scans. In addition to this, we have combined the sensor with a Siemens 1.5T MRI apparatus at Haga Hospital in The Hague. In Figure 14 the results are shown: No disturbances were observed combining the sensor with a fully operational MRI scanner. We are therefore confident that this prototype low-cost FBG pressure cascade sensor, is suitable for further development towards higher TRL levels and could even be developed into a market ready product. Another development in the future will involve the drastic extension of the dynamical properties of the micro fabricated photonic integrated circuit. The interesting development of an on-chip Mach Zehner Interferometer on a chip, resulting into a ultrasonic wave sensor, as explored in the group of Prof. Caro [22], [23] is an interesting candidate for further development. In general, micro structured PICs show great potential due to their immunity to EMI, measuring first of all basic quantities such as temperature and (ultrasonic) pressure in an array, but this may be extended in the future towards measuring oxygen concentration, C-reactive protein concentration, and many more. All micro structured PIC sensors should be developed such, that the can be integrated in catheter tube. In this way a powerful diagnostic tool can be developed in the future. Characteristics and performance of the fabricated cascaded blood pressure sensors were determined by applying various loading conditions and measuring the wavelength shift relative to a steady state at 0 mmHg.

ACKNOWLEDGMENT

Funding provided by the SIA KIEM and SIA MKB-RAAK funding programs. We would like to thank Michiel Oderwald, Martin Lemmen and Wim de Jong from the research groups OptoMechatronics and Optics of TNO High Tech Industry for their valuable contributions to the first phase of this research. We would also like to thank Henk van Zeijl (EKL) for sharing his knowledge and skills – his transfer of knowledge and excellent supervision of many of the THUAS student involved in projects. We would like to thank former Physics students Dorus Elstgeest, Lennart van der Hengel, Huib Dijkstra, Nils Boertjes, Lea Visscher, Iris van der Heide, Esther Pot, Bas Hankel and Basten van der Vorm, Sjoerd Wijgerse for their dedicated experimental work as well as FEM simulations. We also acknowledge Hemanth Ramanna and his team for the allowance to do measurements using the MRI setup at the HagaZiekenhuis, The Hague. We would like to thank the companies Vanderhoek Photonics B.V., Somni Solutions B.V. CD Leycom B.V., Unitron B.V., Delta Life Sciences B.V. Mensure Trading B.V. and Photon First B.V., for their support, supervision and advisory role. We would also like to thank the research laboratories involved for their support, CITC and EKL and TNO, and the research groups of Fontys (Applied Natural Sciences) and Saxion (Applied Nanotechnology). We would also like to thank the IARIA conference organization and jury for rewarding us with Best Paper Award at the ALLSENSORS conference in Venice in 2023. We like to thank the The Pim Breebaart Research Award (PBRA) jury and are grateful for granting the PBRA award in 2023 to this research consortium.

ISSN No. 2454-6194 | DOI: 10.51584/IJRIAS |Volume XI Issue III March 2026

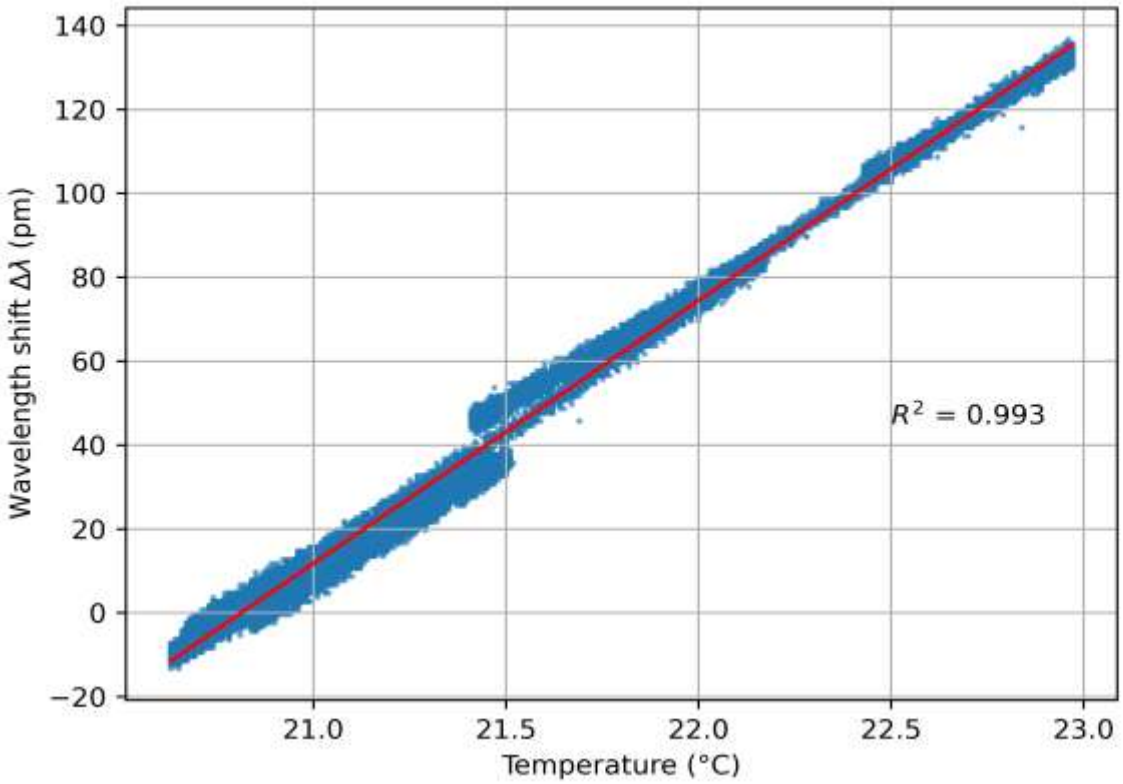

Figure 14. The wavelength shift as a function of temperature. In this measurement, the pressure tubing is disconnected.

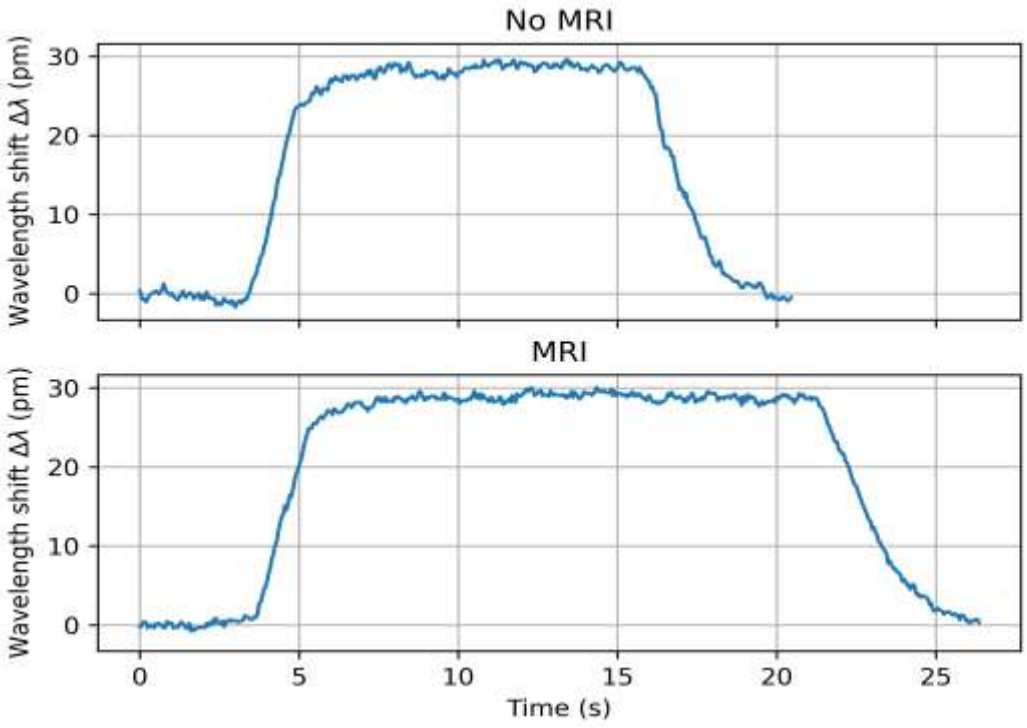

.

Figure 15. A pressure wave (standardized to be equivalent to 30 pm wavelength shift) is applied to the sensor pressure system twice.

REFERENCES

1. L. Arntzen, D. Boesten, et. al., "MRI-Compatible Cascaded Blood Pressure Microsensor", The Eighth International Conference on Advances in Sensors, Actuators, Metering, Pages: 41 to 44, April 24, 2023, Published in: ALLSENSORS 2023, Venice, Italy Copyright (c) IARIA, ISSN: 2519-836X, ISBN: 978-1-68558-083-4083-4.
2. K. O. Hill, et. al., Photo-sensitivity in optical fiber waveguides: application to reflection fiber fabrication", Appl. Phys. Lett. 32 (10): 647, doi:10.1063/1.89881.
3. Campbell et al., "Development of a prototype bridge scour sensor exploiting vortex-induced vibrations", Proceedings of the Institution of Civil Engineers, Bridge Engineering, doi:10.1680/jbren.23.00034.
4. J. W. Arkwright et. al., "Fiber Optic Pressure Sensing Arrays for Monitoring Horizontal and Vertical Pressures Generated by Traveling Water Waves", IEEE Sensors Journal, Vol. 14, No. 8, August 2014.
5. J. W. Arkwright et. al., "In-vivo Demonstration of a High Resolution Optical Fiber Manometry Catheter for Diagnosis of Gastrointestinal Motility Disorders", Optics Expres 4500, Vol. 17, No. 6.
6. Nayak et al., "Enhancing fault detection and predictive maintenance of rotating machinery with Fiber Bragg Grating sensor and machine learning techniques", International Journal of Information Technology, https://doi.org/10.1007/s41870-024-02256-4.
7. J. S. van den Brink, "Concepts in Magnetic Resonance Part B", Review Article, Thermal Effects Associated with RF Exposures in Diagnostic MRI: Overview of Existing and Emerging Concepts of Protection, 17 June 2019, https://doi.org/10.1155/2019/9618680.
8. J. Overgaard, "The heat is (still) on – The past and future of hyperthermic radiation oncology, Radiotherapy and Oncology", Volume 109, ISSUE 2, P185-187, November 2013, DOI: https://doi.org/10.1016/j.radonc.2013.11.004
9. Q. Shao et. al., "Tumor therapeutic response monitored by telemetric temperature sensing, a preclinical study on immunotherapy and chemotherapy", Scientific Reports volume 13, Article number: 7727 (2023)
10. A. R. Niknam, S. Dodge, M. Hajian and M. A. Ansari, "Characterization of microwave heating for hyperthermia cancer treatment". Waves in Random and Complex Media, 34(1), 211–225, https://doi.org/10.1080/17455030.2021.1905911.
11. Ioannis Androulakis a, Rob M.C. Mestrom b, Sergio Curto Inger-Karine K. Kolkman-Deurloo a, Gerard C. van Rhoon, "Pre-clinical prototype validation and characterization of a thermo-brachytherapy system for interstitial hyperthermia and high-dose rate brachytherapy", Physics and Imaging in Radiation Oncology,https://doi.org/10.1016/j.phro.2024.100606
12. David M. Smadja, "Hyperthermia for Targeting Cancer and Cancer Stem Cells: Insights from Novel Cellular and Clinical Approaches", Stem Cell Reviews and Reports, https://doi.org/10.1007/s12015-024-10736-0
13. M. Szwed, A. Marczak, "Application of Nanoparticles for Magnetic Hyperthermia for Cancer Treatment", The Current State of Knowledge, Cancers 2024, 16(6), 1156; https://doi.org/10.3390/cancers16061156.
14. Heart Foundation, "Cardiovascular diseases in the Netherlands 2021", https://hartstichting-hartstichting-portal-p01.s3.eu-central-1.amazonaws.com/s3fs-public/2022-11/hart-en-vaatziekten-nederland-cijfers-2021.pdf?, [retrieved: March, 2026].
15. K. Peels, N. H. J. Pijls, B. de Bruyne. "Measurement of fractional flow reserve to assess the functional severity of coronary-artery stenoses", New English Journal of Medicine, June 1996.
16. Ł. Dziuda, M. Krej and F. W. Skibniewski, "Fiber Bragg Grating Strain Sensor Incorporated to Monitor Patient Vital Signs During MRI," in IEEE Sensors Journal, vol. 13, no. 12, pp. 4986-4991, doi: 10.1109/JSEN.2013.2279160.
17. A. Kumar, D. J. Patton, M. G. Friedrich, "The emerging clinical role of cardiovascular magnetic resonance imaging", Jun 2010, publisher: Pulsus Group
18. UMC Utrecht,"7T-MRI", https://www.umcutrecht.nl/nl/wetenschappelijk-onderzoek/7t-mri, [retrieved: March 2026].https://en.wikipedia.org/wiki/Venturi_effect [retrieved: March 2026].
19. J. E. Hall, "Guyton and Hall Textbook of Medical Physiology", pp. 155-166, 2003.

20. M. F. O'Rourke, "Time domain analysis of the arterial pulse in clinical medicine", Med Biol Eng Comput 47, pp. 119–129, Feb 2009, publisher: IFMBE.
21. B. Uyang et. al., Integrated photonics Interferometric Interrogator for a Ring-Resonator Ultrasound Sensor, OPTICS EXPRESS 23408, Vol. 27, No. 16, 5 Aug 2019.
22. B. Uyang et. al., On-chip silicon Mach–Zehnder Interferometer, Sensor for Ultrasound Detection, Optics Letters, Vol. 44, No. 8, 15 April 2019.
23. FBGS, Draw Tower Gratings, Overview, https://fbgs.com/components/draw-tower-gratings-dtgs/, retrieved: March 2026.
24. Femto Sensing International, FAZT I4G INTERROGATOR Datasheet, https://femtosensing.com/wp-content/uploads/2020/01/ FSI-FAZ-I4G-Interrogator-Datasheet-V4.pdf, retrieved: Feb 2023.
25. Norland Products, Norland Optical Adhesive 65 Technical Datasheet, https://norlandproducts.com/adhesives, [retrieved: March 2026].
26. COMSOL Multiphysics® V5.6 https://www.comsol.com, [retrieved: March 2026.